THE JOURNAL OF PHYSICAL CHEMISTRY C

Article

Cite This: J. Phys. Chem. C 2019, 123, 19927−19937

pubs.acs.org/JPCC

Temperature-Dependent Electroabsorption and Electrophotoluminescence and Exciton Binding Energy in $MAPbBr_3$ Perovskite Quantum Dots

Shailesh Rana,[†] Kamlesh Awasthi,[†] Sumit S. Bhosale,[†] Eric Wei-Guang Diau,*[,†,‡] and Nobuhiro Ohta*[,†,‡]

[†]Department of Applied Chemistry and Institute of Molecular Science and [‡]Center for Emergent Functional Matter Science, National Chiao Tung University, 1001 Ta-Hsueh Rd., Hsinchu 30010, Taiwan

Supporting Information

ABSTRACT: Organic−inorganic lead halide perovskite nanocrystals have attracted much attention as promising materials for the development of solid-state light-emitting devices, but the existence of free or bound excitons or the formation of trap states remains under debate. We recorded the temperature-dependent electroabsorption (E-A) and electrophotoluminescence (E-PL) spectra, that is, electric-field-induced change in absorption and photoluminescence spectra, for methylammonium lead tribromide ($MAPbBr_3$) colloidal perovskite nanocrystals, that is, quantum dots (QD), doped in a poly(methyl methacrylate) film in the temperature range of 40−290 K. Based on the results, the binding energy of the exciton (electron−hole pair) was estimated. The exciton binding energy of QD of $MAPbBr_3$ estimated from the absorption and E-A spectra (∼17 meV) is nearly the same as that of a $MAPbBr_3$ polycrystalline thin solid film, while the exciton binding energy estimated from the temperature-dependent PL spectra (∼70 meV) is much greater than that estimated from the absorption profile. The frequency dependence of the E-A intensity observed at 40 and 290 K for the modulated applied electric field indicates a slow ion migration in nanocrystals, which follows the modulation of the applied electric field at a frequency less than 500 Hz. The observed E-A spectra were analyzed with an integral method on assuming the Stark effect; the magnitudes of the changes in electric dipole moment and polarizability following photoexcitation were determined at each temperature from 40 to 290 K. E-PL spectra show that the PL of QD of $MAPbBr_3$ is quenched on the application of an external electric field; the extent of quenching is much greater for trap emission than for exciton emission. Exciton−phonon scattering, which is responsible for the line broadening of the PL spectra, is also discussed based on the temperature-dependent PL spectra.

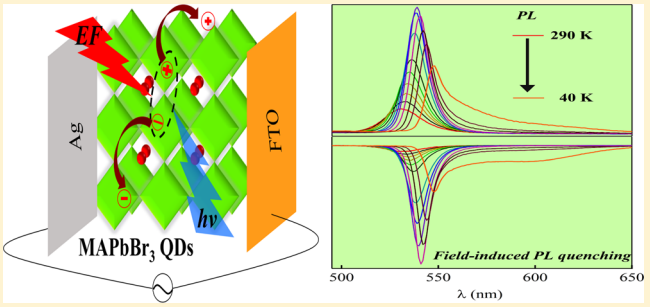

INTRODUCTION

Hybrid organic−inorganic lead halide perovskites have become one of the most interesting and most studied materials in recent years with respect to their applications in optoelectronic functional devices, such as photovoltaic cells, memory devices, photodetectors, and light-emitting devices (LED).[1−6] Their unique optical and electronic properties, such as a tunable band gap, broad range of absorption, tunable emission in the visible region, and photon recycling make them promising materials for future prospects.[7−11] Moreover, ferroelectric properties, intrinsic defects, thermal conductivity, and charge migration due to the internal or external electric fields in perovskite materials play a versatile role in optoelectronic devices.[12−16]

Besides the bulk perovskite materials, semiconductor nanocrystals have inspired a vital research area for energy materials because of the quantum-confinement effect, which typically leads to a large binding energy of an exciton as well as the variation of their tunable optical properties and a large quantum yield (QY) for emission.[10,17−19] Because of the outstanding optoelectronic characteristics of organic−inorganic lead halide perovskites (PSK), nanometer-sized methylammonium lead tribromide perovskite nanocrystals, that is, QD (abbreviated as $MAPbBr_3$:QD), which showed intense emission and a large QY for LED, were reported by Schmidt et al.[17] to extend the evolution of the PSK family into a new era of nanotechnology.[20−23] Despite the intensive attention to intrinsic properties within $MAPbBr_3$:QD, it is still unclear whether only bound excitons are created or free charges are spontaneously generated in $MAPbBr_3$ nanomaterials and whether there exists scattering induced by the electron−phonon interaction and self-trap formation.[24−26] These are critical problems that remain subject to debate in $MAPbBr_3$:QD; it is important to elucidate the electronic

Received: May 14, 2019
Revised: July 9, 2019
Published: August 1, 2019

DOI: 10.1021/acs.jpcc.9b04567
J. Phys. Chem. C 2019, 123, 19927−19937

structure and dynamics that cause the characteristic absorption and PL properties of these nanomaterials. Electron−phonon coupling, defect, and self-trapping, which generally depend on the temperature, pressure, crystal structure, and electric field,[26−31] are disadvantageous for both the photovoltaic and LED applications, because these physical parameters affect the carrier mobility and induce a line broadening in the PL spectra. It is hence important to clarify these physical properties of $MAPbBr_3$:QD from the points of view of both fundamental and applied research.

An external electric field has been extensively applied to illuminate a working mechanism of organic dye-sensitized solar cells (DSSC) and in perovskite-based photovoltaic cells and to modulate the excited-state dynamics, including charge transfer, in $MAPbI_3$ and $(C_4H_9NH_3)_2PbI_4$ organic−inorganic quantum wells.[27,28,32−34] With increasing temperature, various phenomena, including thermal dissociation of excitons and electron−phonon scattering, affect the optical properties, such that detailed information regarding exciton dynamics of materials cannot be readily obtained from only the experiments of absorption and PL near 300 K.

We have recorded the temperature-dependent E-A and E-PL spectra of $MAPbBr_3$:QD doped in a poly(methyl methacrylate) (PMMA) film to probe the charge carrier dynamics, electron−phonon scattering, and trap emission, devoting particular attention to the estimation of the exciton binding energy of $MAPbBr_3$:QD. Slow ion migration is also discussed based on an E-A signal obtained with varied modulation frequencies of the applied electric field. Electron−phonon scattering, the formation of self-trapped excitons, and effects of an external electric field on the photoexcitation dynamics of $MAPbBr_3$:QD doped in a PMMA film are also discussed, based on the measurements of temperature-dependent PL and E-PL spectra.

EXPERIMENTAL SECTION

Sample Preparation of $MAPbBr_3$ Quantum Dots. $MAPbBr_3$:QD were synthesized with the reported top-down method.[19] CH_3NH_3Br (Dyesol, 8 mmol) and $PbBr_2$ (Alfa Aesar, 8 mmol) were mixed in oleic acid (Aldrich, 40 mL) and oleylamine (Aldrich, 4 mL) in a centrifuge tube. The mixture was sonicated for 4 days. During sonication, the bulk perovskite was formed first as a precursor, from which further sonication broke down the bulk perovskite into nanoparticles, that is, QD, each of which was protected with oleic acid and oleylamine. The synthesized QDs were collected on centrifugation and dispersed in toluene for further purification. The toluene solution of QD was centrifuged five times; the final supernatant was collected in toluene (10 mL).

Sample Preparation for E-A and E-PL Measurements. To prepare the solid film for the measurements of E-A and E-PL spectra, we cast a selected volume of toluene solution of a mixture of $MAPbB_3$:QD and PMMA on fluorine-doped tin oxide (FTO)-coated glass substrate with a spin-coating method. The typical thickness of the prepared film of $MAPbB_3$:QD doped in a PMMA film was ∼0.4 μm, determined with an alpha step method (Veeco Dektak 150); a semitransparent aluminum (Al) film of ∼15 nm in thickness was then deposited by thermal evaporation on the prepared PMMA film that includes $MAPbBr_3$:QD. The FTO and Al films served as electrodes; the field strength was evaluated from the applied voltage divided by the distance between electrodes.

E-A and E-PL Spectra at Varied Temperatures. All spectra were recorded under vacuum conditions at each temperature in the range of 40−290 K using a cryogenic refrigerator (Daikin, V202C5LR), which had silica optical windows, and a temperature controller (Scientific Inst., model 9600-1) with a silicon-diode thermometer to control the substrate temperature. Steady-state absorption and PL spectra were recorded with a spectrometer (JASCO, FP-777). Electric-field modulation spectroscopy was applied to measure E-A and E-PL spectra with the same apparatus as described elsewhere.[35] A sinusoidal ac voltage with a modulation frequency in the range of 40 Hz to 1 kHz was applied to modulate the transmitted light of the excitation (I_{EX}) or PL intensity (I_{PL}). A field-induced change in the transmitted intensity (ΔI_{EX}) or the PL intensity (ΔI_{PL}) was detected with a lock-in amplifier at the second harmonic of the modulation frequency. The dc component of I_{EX} or I_{PL} was concurrently recorded with a computer. E-A spectra and E-PL spectra were derived on plotting the field-induced change of absorbance $\Delta A(\equiv \left(\frac{\Delta I_{EX}}{I_{EX}}\right)\log e)$ and the field-induced change of PL intensity (ΔI_{PL}), respectively, as a function of wavelength or wavenumber.

RESULTS AND DISCUSSION

Sample Characterization. A TEM image and the size distribution of $MAPbBr_3$:QD prepared in the present work, which yields an average size of particles about 6 nm, are shown in Figure 1, which also shows the XRD patterns of the synthesized sample as a function of temperature, crystallographic information file (CIF) of $MAPbBr_3$:QD, and corresponding cubic crystal structure.[36] A typical TEM image of a single QD of $MAPbBr_3$ is also shown in Figure S1, Supporting Information.

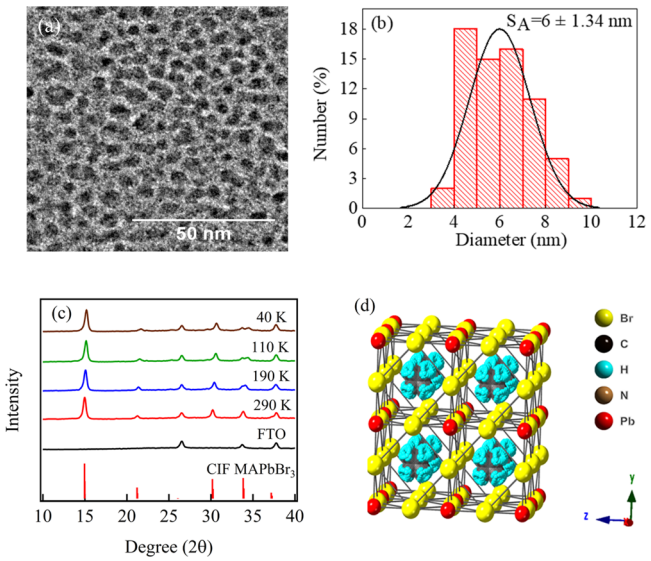

Figure 1. (a) TEM image, (b) size distribution, which shows an average diameter (S_A) of 6 nm, (c) XRD patterns at varied temperatures, and (d) cubic crystal structure of quantum dots (QD) of $MAPbBr_3$, that is, $MAPbBr_3$:QD. The XRD pattern of FTO and crystallographic information file (CIF) of $MAPbBr_3$ are also shown in (c).

DOI: 10.1021/acs.jpcc.9b04567
J. Phys. Chem. C 2019, 123, 19927−19937

Absorption and Electroabsorption (E-A) Spectra. Figure 2a shows the temperature-dependent absorption spectra

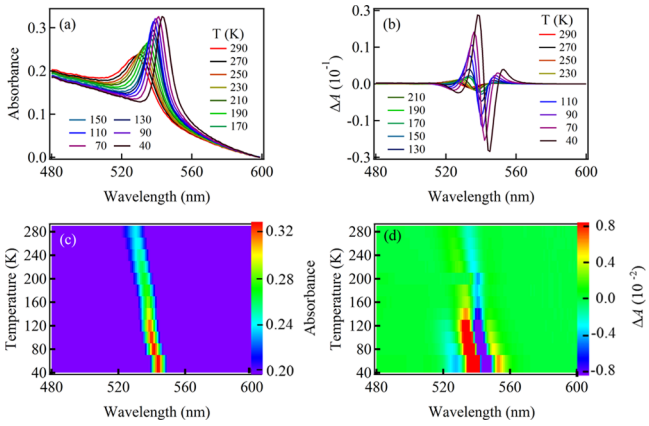

Figure 2. (a) Absorption and (b) E-A spectra of $MAPbBr_3$:QD doped in a PMMA film recorded at varied temperatures and (c, d) their temperature-resolved intensity images, respectively. E-A spectra were recorded with an applied electric field with a strength of 0.4 MV cm^{-1}.

of $MAPbBr_3$:QD doped in a PMMA film observed from 40 to 290 K with a temperature-resolved intensity image of the absorption spectra. Along with the continuous free carrier absorption in the higher energy region, a prominent exciton absorption feature was observed at every temperature measured in the range of 40−290 K. The absorption tail extending to a region of wavelength greater than the exciton band is caused by scattering. With decreasing temperature, the main exciton absorption feature shifted monotonically from 528 ± 3 nm at 290 K to 544 ± 3 nm at 40 K; the peak intensity increased (see Figure 2a,c). Near 296 K, the main exciton band was assigned to the intra-atomic transition from 6s to 6p orbital in Pb^{2+}.[37] The red shift of the exciton signal with decreasing temperature is similar to that of other lead composite semiconductors.[26,38−41] The position of the exciton absorption of $MAPbBr_3$:QD in a PMMA film at 290 K is similar to that of the exciton absorption of a polycrystalline thin solid film of $MAPbBr_3$, that is, 530 nm.[34] As the XRD patterns in Figure 1 show, the temperature-dependent shift and change in absorption intensity do not arise from a phase transition in the crystal structure of $MAPbBr_3$:QD; the cubic structure of $MAPbBr_3$:QD persists in the entire temperature range of 40−290 K, in contrast with a $MAPbBr_3$ polycrystalline thin film or a single crystal, which was reported to show a phase transition,[42,43] but the Bragg peaks shifted monotonically to a greater diffraction angle with decreasing temperature, indicating a lattice contraction.

The red shift of the exciton absorption feature with decreasing temperature, i.e., a decreased band-gap energy (E_g), which is shown in Figure S2, Supporting Information, differs from that of conventional semiconductors, which show a blue shift on decreasing temperature, as a result of lattice contraction. In conventional semiconductors, the valence-band maxima (VBM) and conduction-band minima (CBM) arise from bonding and antibonding orbitals in pairs. In the results, the band gap between the VBM and the CBM increases with lattice contraction.[44,45] In lead halide perovskites, in contrast, the VBM and CBM are formed from an antibonding orbital between Pb(s)-Br(p) and Pb(p)-Br(p), respectively; the potential energy of VBM and CBM hence alters through the thermal contraction of the lattice, leading to an energy of the band gap decreasing with decreasing temperature.[28,38,46]

Figure 2b,d shows that the E-A spectra of $MAPbBr_3$:QD in a PMMA film also depend on the temperature; the intensity of the E-A spectra increased monotonically with decreasing temperature. Figure 3 shows plots of the E-A intensity

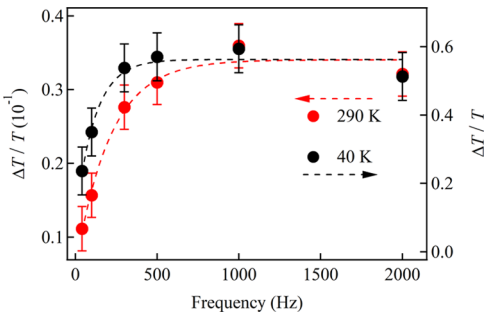

Figure 3. Frequency dependence of field-induced variation of absorption intensity, that is, field-induced variation of transmitted intensity of excitation light relative to the intensity transmitted at zero field, that is, $\Delta T/T$, at 290 K (red circle) and 40 K (black circle). Plots of $\Delta T/T$ as a function of the modulation frequency of the applied electric field were obtained with a field strength of 0.4 MV cm^{-1} at the maximum intensity of the E-A signal.

observed at 40 and 290 K with a field strength 0.4 MV cm^{-1} as a function of modulation frequency of the applied electric field; the E-A intensity depends on the frequency of the applied electric field. The E-A signal, which is weak at low frequencies, increased with increasing modulation frequency and saturated at frequencies greater than 500 Hz at both 40 and 290 K. The frequency dependence of the E-A intensity is considered to result from an electric-field-induced ion migration in $MAPbBr_3$:QD. The phenomenon of slow ion migration was reported for a film of small $MAPbI_3$ perovskite nanocrystals.[15,16] Although the average particle size of $MAPbBr_3$:QD in the present samples is as small as 6 nm (see Figure 1b), slow ion migration is considered to occur inside the QD of $MAPbBr_3$ following the modulation of the applied electric field. The frequency-dependent E-A signals saturated at a lower frequency at 40 K than at 290 K (Figure 3), indicating that the field-induced ion migration becomes more efficient with increasing temperature. To avoid the influence of ion migration, E-A spectra shown in Figure 2 and E-PL spectra, to be presented, were obtained at each temperature with a modulation frequency of 1 kHz of the applied electric field, unless otherwise noted. These spectra were reproducible, indicating that the sample of $MAPbBr_3$:QD was stable on the application of such a strong field of 0.4 $MVcm^{-1}$.

Figure 4 shows the E-A spectra of $MAPbBr_3$:QD in a PMMA film observed with field strengths varied from 0.1 to 0.4 MV cm^{-1} at 40 and 290 K. E-A signals of $MAPbBr_3$:QD in a PMMA film observed at the maximum (18,587 cm^{-1}) and minimum (18,382 cm^{-1}) at 40 K and at the maximum (19,157 cm^{-1}) and minimum (18,726 cm^{-1}) at 290 K are proportional to the square of the applied electric field. The crossing point at 18,948 cm^{-1} at 290 K and at ~18,492 cm^{-1} at 40 K remained unchanged (Figure 4a and b). These results indicate that, in principle, the observed E-A signals arise from the Stark shift, but it is admitted that an abnormal behavior inexplicable in terms of a simple Stark shift was also observed at low

DOI: 10.1021/acs.jpcc.9b04567
J. Phys. Chem. C 2019, 123, 19927−19937

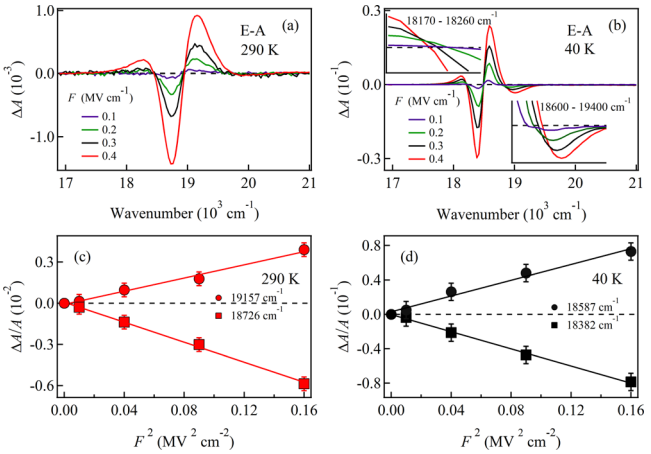

Figure 4. E-A spectra of $MAPbBr_3$:QD observed with varied applied electric-field strengths at (a) 290 K and (b) 40 K; plots of the dependence of the applied field strength of $\Delta A/A$ as a function of the squared field strength observed at the maximum and minimum signals of ΔA at (c) 290 K and (d) 40 K. Inset figures in (b) show an extended view for two parts of the E-A spectra at 40 K, that is, from 18,170 to 18,260 cm^{-1} and from 18,600 to 19,400 cm^{-1}.

temperatures. An extended view of the E-A signal at 40 K between 18,170 and 18,260 cm^{-1} and between 18,600 and 19,400 cm^{-1}, shown in Figure 4b (inset), indicates that the zero-crossing points of the E-A spectrum show a red shift and a blue shift, respectively, with increasing field strength. A similar shift, dependent on field strength, of the zero-crossing point was reported by Amerling et al., for the E-A spectra of the exciton and continuum bands of two-dimensional butylammonium lead iodide $(C_4H_9NH_3)_2PbI_4$ quantum wells.[27] The shift of the zero-crossing point observed only at low temperatures was interpreted in terms of a Franz−Keldysh (FK) oscillation of the continuum band. As the origin of the present field strength-dependent shift of the zero-crossing point in the E-A spectra of $MAPbBr_3$:QD, the FK oscillation is one possibility, although it is uncertain whether the oscillation can appear in regions of both large and small energy of the exciton absorption signal. As another possible origin of the field strength-dependent shift of the zero crossing, a field-induced deformation of the crystal lattice might be considered, because a deformation of the crystal lattice induced on the application of an electric field might lead to a shift of the absorption edge.[47] In the results, the E-A spectra of $MAPbBr_3$:QD in a PMMA film at low temperatures are explicable in terms of a Stark shift and a small contribution of the FK oscillation or a field-induced lattice deformation.

In the Stark shift, the energy level of the absorption band is shifted by $-\Delta\boldsymbol{\mu}F - \Delta\boldsymbol{\alpha}F^2/2$ on the application of an external electric field (F); $\Delta\boldsymbol{\mu}$ and $\Delta\boldsymbol{\alpha}$ represent the differences of electric dipole moment and polarizability, respectively, between the excited state (e) and ground state (g), that is, $\Delta\boldsymbol{\mu} = \boldsymbol{\mu}_e - \boldsymbol{\mu}_g$ and $\Delta\boldsymbol{\alpha} = \boldsymbol{\alpha}_e - \boldsymbol{\alpha}_g$. In an isotropic sample, the field-induced change in absorption intensity at wavenumber ν, that is, $\Delta A(\nu)$, is given by the zeroth, first, and second derivatives of the absorption intensity $A(\nu)$ in a linear combination as follows:[48−51]

$$\Delta A(\nu) = (fF)^2\left[A_\chi A(\nu) + B_\chi \nu \frac{d}{d\nu}\left(\frac{A(\nu)}{\nu}\right) + C_\chi \nu \frac{d^2}{d\nu^2}\left(\frac{A(\nu)}{\nu}\right)\right] \quad (1)$$

where f represents the internal field factor and $F = |\boldsymbol{F}|$. The value of A_χ depends on the field-induced change in the transition moment, and coefficients B_χ and C_χ pertain to the spectral shift and spectral broadening of absorption, respectively. These coefficients are used to calculate the magnitude of $\Delta\boldsymbol{\mu}$ and $\Delta\boldsymbol{\alpha}$ as

$$B_\chi = \frac{\Delta\bar{\alpha}}{2hc},\quad C_\chi = \frac{|\Delta\boldsymbol{\mu}|^2}{6h^2c^2} \quad (2)$$

in which $\Delta\bar{\alpha}$ denotes the trace of $\Delta\boldsymbol{\alpha}$, that is, $\Delta\bar{\alpha} = (1/3)\mathrm{Tr}(\Delta\boldsymbol{\alpha})$.

In the present absorption spectra of $MAPbBr_3$:QD, the exciton band, the continuum band, and the absorption tail caused by the scattering overlap each other severely; separation into each band is difficult. In such a condition, an integral method is useful for the analysis of the E-A spectra.[52,53] Scattered light typically exhibits no electric field effect. If an E-A spectrum is expressed with eq 1, then the integral of an E-A spectrum along the wavenumber becomes

$$\int \Delta A(\nu) \cong (fF)^2\left[A_\chi \int A(\nu)d\nu + B_\chi A(\nu) + C_\chi \frac{dA(\nu)}{d\nu}\right] \quad (3)$$

Further integration of eq 3 over the wavenumber, that is, a second integral of E-A spectra, becomes

$$\int\left\{\int \Delta A(\nu)d\nu\right\}d\nu \cong (fF)^2\left[A_\chi \int\left\{\int A(\nu)d\nu\right\}d\nu + B_\chi \int A(\nu)d\nu + C_\chi A(\nu)\right] \quad (4)$$

The first and second terms on the right side of eq 4 show a monotonic increase or decrease, depending on A_χ and B_χ, whereas the third term imposes a spectral shape that is the same as the absorption spectrum.

Simulation of not only the E-A spectra but also their first and second integral spectra yields reliable values of A_χ, B_χ, and C_χ. The results of the simulation with the integral method are shown in Figure 5 for the E-A spectra at 290 and 40 K and in Figures S3−S6, Supporting Information for the E-A spectra recorded at other temperatures. Based on the analysis, the magnitudes of $|\Delta\boldsymbol{\mu}|$ and $\Delta\bar{\alpha}$ have been estimated at each temperature, as shown in Figure 6. $|\Delta\boldsymbol{\mu}|$ is ∼4 D, and $\Delta\bar{\alpha}$ is approximately −100 $Å^3$ at 290 K; these values remained similar at temperatures above 150 K, whereas the magnitudes of both $|\Delta\boldsymbol{\mu}|$ and $\Delta\bar{\alpha}$ increased with the temperature decreasing below 150 K, reaching ∼10 D and −1070 $Å^3$ at 40 K, respectively, as shown in Figure 6. E-A spectra in the higher wavenumber region were irreproducible at low temperatures, for example, at 40 K, as shown in Figure 5d, likely because of the presence of FK oscillation, field-induced lattice distortion, or the presence of an unknown weak absorption band. The magnitudes of $|\Delta\boldsymbol{\mu}|$ and $\Delta\bar{\alpha}$ of a $MAPbBr_3$ polycrystalline thin film are reported to be 2.2 D and −4.1 $Å^3$, respectively, near 296 K.[34] The

DOI: 10.1021/acs.jpcc.9b04567
J. Phys. Chem. C 2019, 123, 19927−19937

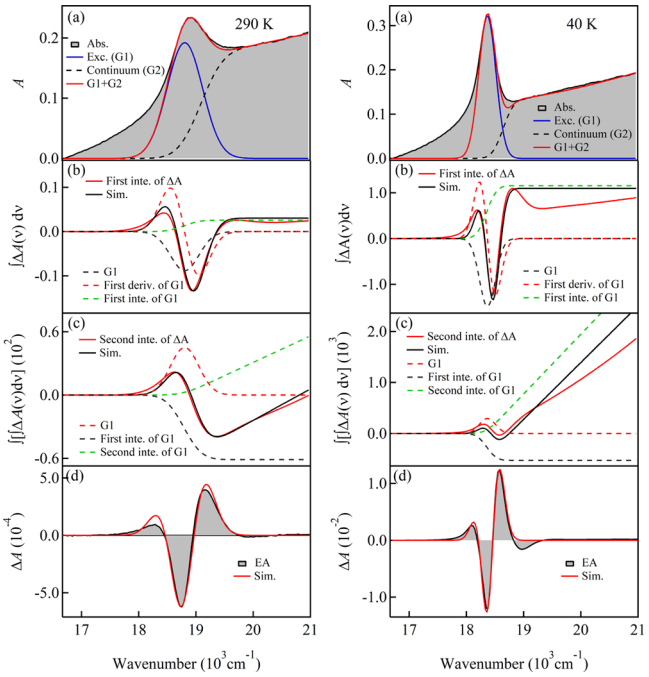

Figure 5. Integral method of analysis of the E-A spectra of $MAPbBr_3$:QD observed at 290 K (left) and 40 K (right). (a) Absorption spectrum (shaded line) and simulated spectrum (red line) given as a sum of the exciton absorption band (G1, blue line) and the continuum absorption (G2, black dotted line), (b) first integral of the E-A spectrum (red solid line), simulated spectrum (black solid line), and each spectrum that contributes to the simulated spectrum, (c) second integral of the E-A spectrum (red solid line), simulated spectrum (black solid line), and each spectrum that contributes to the simulated spectrum, and (d) E-A spectrum (shaded line) observed with a field strength of 0.4 MV cm^{-1} and the simulated spectrum (red solid line).

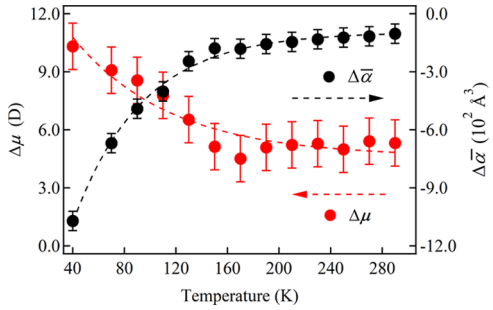

Figure 6. Plots of $|\Delta\mu|$ and $\Delta\bar{\alpha}$ following the absorption of the exciton band of $MAPbBr_3$:QD doped in a PMMA film as a function of temperature, determined with the integral method analysis of the E-A spectra.

magnitudes of both $|\Delta\mu|$ and $\Delta\bar{\alpha}$ in $MAPbBr_3$:QD are much larger than those for a $MAPbBr_3$ polycrystalline thin film, which might arise from a disparate crystal size of $MAPbBr_3$ or a quantum-confinement effect in $MAPbBr_3$:QD. As the type of crystal structure of $MAPbBr_3$:QD remains unchanged with decreasing temperature, the observed temperature-dependent electronic property might arise from the temperature-dependent lattice distortion.

Photoluminescence (PL) and Electrophotoluminescence (E-PL) Spectra. Both PL and E-PL spectra of $MAPbBr_3$:QD doped in a PMMA film were recorded in the temperature range of 40−290 K; the results are shown in Figure 7, in which temperature-resolved intensity images of both PL and E-PL spectra also appear. Both PL and E-PL spectra depend remarkably on the temperature. The spectra of the ratio of the E-PL spectrum and the PL spectrum, that is, plots of the field-induced change in the PL intensity relative to PL intensity as $\Delta I_{PL}/I_{PL}$, as a function of wavelength, and the temperature-resolved intensity images are also shown in Figure 7. The PL and E-PL spectra were recorded concurrently at each temperature. A sharp exciton line is observed in the PL spectra at any temperature; a shoulder peak was also observed in the wavelength region greater than that of the exciton band at low temperatures, for example, 40 K. The PL exciton line shows a monotonic red shift with decreasing temperature, as in the case of the temperature dependence of the exciton absorption signal (see Figures 2c and 7d). For example, the PL exciton maximum is located at 530 nm at 290 K and at 548 nm at 40 K. The exciton peak intensity increased with the temperature decreasing from 290 to 140 K but decreased with the temperature decreasing further from 140 to 40 K. The total intensity integrated over the entire spectral region similarly increased with the temperature decreasing from 290 to 140 K. With further decreasing temperature, of the integrated intensity decreased and then increased at 40 K. The PL intensity observed at 607 nm remained constant at temperatures above 100 K but increased monotonically with the temperature decreasing below 100 K. Plots of PL intensity at the exciton peak, PL intensity at 607 nm, and integrated intensity of PL in the entire spectral region as a function of temperature are shown in Figure S7, Supporting Information.

Temperature-dependent PL spectra of $MAPbBr_3$ were reported by Woo et al. for a single crystal, a polycrystalline thin film, and quantum dots, which probably correspond to the present sample of $MAPbBr_3$:QD.[26] The PL emission maximum was reported to show a blue shift with increasing temperature in every case, in agreement with the present temperature dependence of the exciton peak position of $MAPbBr_3$:QD. These authors also mentioned that multipeak emissions were observed at low temperatures for a thin film and a single crystal but not for quantum dots. In their work, the multipeak PL emissions of a $MAPbBr_3$ thin film and a single crystal at low temperatures were attributed to free excitons and bound excitons trapped at shallow energy defects before recombination, respectively. In contrast with the quantum dots reported by Woo et al., our $MAPbBr_3$:QD show multipeak emissions at low temperatures; the emission intensity near 600 nm relative to the main exciton peak intensity increased with decreasing temperature below 100 K, as mentioned above. As shown in the XRD patterns (Figure 1c), no crystal phase transition was observed for $MAPbBr_3$:QD in the temperature range of 40−290 K, but the PL was observed to extend to a wavelength region longer than that of the exciton band, which is assignable to the emission of bound excitons. As mentioned below, PL emissions of a free exciton and a bound exciton, which are hereafter called exciton emission and trap emission, respectively, show disparate effects of the electric field.

According to Woo et al.,[26] the PL of a thin film or a single crystal of $MAPbBr_3$ decreased rapidly with increasing temperature, whereas the PL intensity of the QD of $MAPbBr_3$ exhibited no such rapid decrease with increasing temperature. In that sense, the temperature dependence of the PL intensity of $MAPbBr_3$:QD is similar to that of the QD of $MAPbBr_3$,[26] for which the PL intensity was reported near 296 K to be about

DOI: 10.1021/acs.jpcc.9b04567
J. Phys. Chem. C 2019, 123, 19927−19937

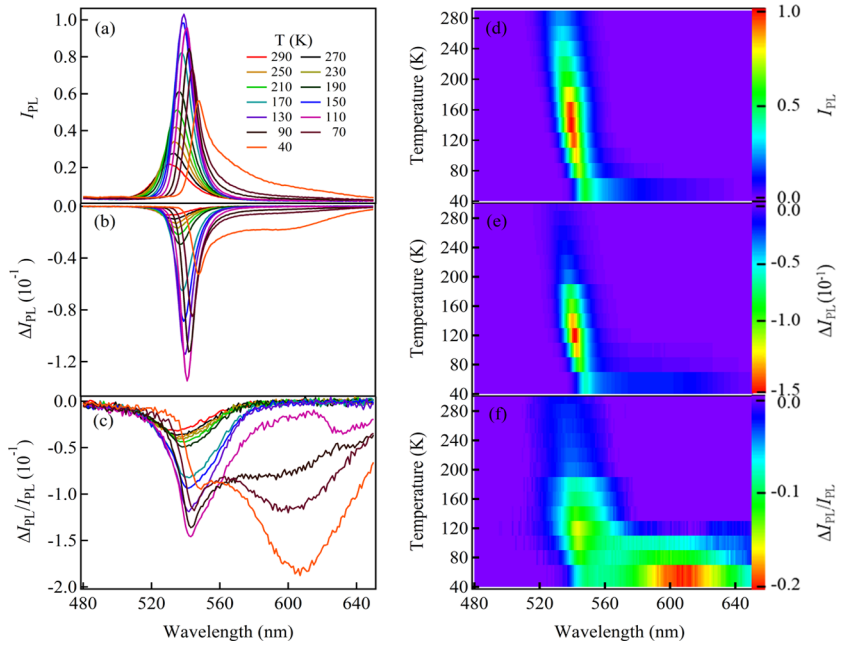

Figure 7. (a) PL spectra, (b) E-PL spectra, and (c) the ratio between E-PL and PL spectra, that is, the spectra of $\Delta I_{PL}/I_P$ of $MAPbBr_3$:QD doped in a PMMA film observed at varied temperatures. Their temperature-resolved intensity images are shown in the right. E-PL spectra were recorded with a field strength of 0.1 MV cm^{-1}. The excitation wavelength was 420 nm.

40% of the maximum intensity at low temperatures. In the present samples, the integrated intensity at 290 K is about half the integrated intensity at 140 K, at which the maximum intensity was observed (see Figure S7, Supporting Information). The present results for the temperature dependence of the peak intensity of the exciton band, integrated intensity, and intensity at 607 nm show that the population of the exciton decreased with decreasing temperature below 140 K, resulting in increased trap emission and a decreased exciton emission with decreasing temperature.

The exciton PL band became narrower with decreasing temperature from 290 K. The PL bandwidth is generally affected by the electron−phonon (E-P) interaction, so that the strength of the E-P interaction can be estimated from the PL bandwidth. The temperature (T)-dependent PL bandwidth is expressed as[26,40,54,55]

$$\Gamma(T) = \Gamma_0 + \Gamma_{ac} + \Gamma_{LO} + \Gamma_{imp} = \Gamma_0 + \gamma_{ac}T + \gamma_{LO}N_{LO}(T) + \gamma_{imp}e^{-E_b/k_BT} \quad (5)$$

Here, Γ_0, Γ_{ac}, Γ_{LO}, and Γ_{imp} represent the temperature-independent inhomogeneous linewidth at 0 K, the homogeneous broadening due to the acoustic phonon scattering, the homogeneous broadening due to LO phonon scattering, and the inhomogeneous broadening due to ionized impurities of average binding energy E_b, respectively. γ_{ac} and γ_{LO} are the coupling strengths between exciton and acoustic phonon and between exciton and optical phonon, respectively. In general, exciton−phonon coupling is proportional to the occupation number of the phonons, $N_{LO}(T)$, described with the Bose−Einstein distribution: $N_{LO}(T) = \frac{1}{[e^{E_{LO}/k_BT} - 1]}$, in which E_{LO} is the phonon energy and k_B is the Boltzmann constant. At temperatures below 100 K, the contribution of optical phonons is small; the bandwidth was hence fitted with Γ_0 and accoustic phonon scattering (Γ_{ac}). Plots of bandwidth of the exciton band in the recorded PL spectra of $MAPbBr_3$:QD are shown in Figure 8, as a function of temperature. The temperature

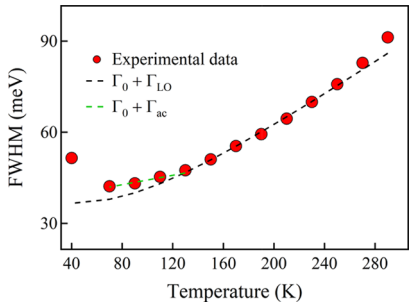

Figure 8. Bandwidth of the exciton PL band (FWHM) of $MAPbBr_3$:QD doped in a PMMA film as a function of temperature with curves fitted with eq 5. The black dashed line shows the combination between inhomogeneous broadening and the bandwidth caused by an LO phonon (E_{LO} = 25 meV); the green dashed line shows the combination between inhomogeneous broadening and the bandwidth caused by an acoustic phonon.

dependence of the bandwidth of the exciton PL band was simulated with eq 5 employing E_{LO}=25 meV, γ_{LO} = 85.1 meV, and γ_{ac} = 0.9 meV. These values of E_{LO} and γ_{LO} are similar to those reported by Woo et al., that is, 24.9 and 80.1 meV, respectively; the value of γ_{ac} is much smaller than the reported 6.3 meV.[26]

Temperature-dependent E-PL spectra shown in Figure 7b indicate that the PL of $MAPbBr_3$:QD doped in a PMMA film is quenched on the application of an electric field at any temperature in the range of 40−290 K; the emission quantum yield hence decreases in the presence of an electric field at any temperature. The E-PL spectra were recorded with excitation at 420 nm, at which the field-induced change in absorption intensity was negligible. The spectra of $\Delta I_{PL}/I_{PL}$ at 290 and 40 K are also shown in Figure 9 with I_{PL} and ΔI_{PL} spectra. As

DOI: 10.1021/acs.jpcc.9b04567
J. Phys. Chem. C 2019, 123, 19927−19937

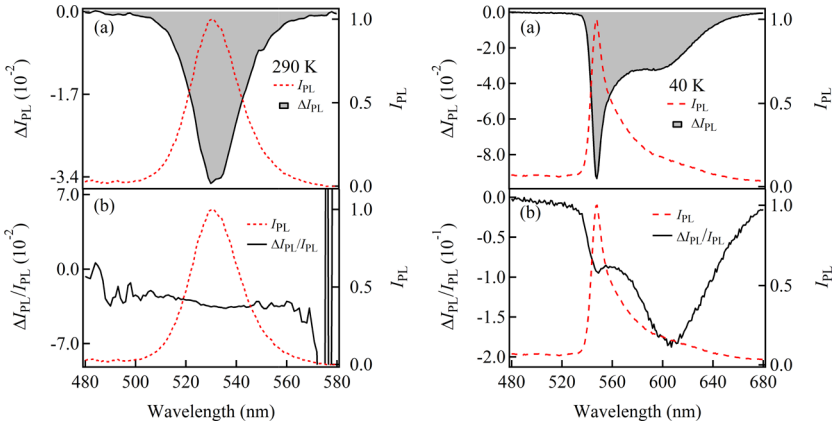

Figure 9. (a) PL and E-PL spectra of $MAPbBr_3$:QD doped in a PMMA film observed at 290 K (left) and at 40 K (right) with excitation at 420 nm and (b) PL and $\Delta I_{PL}/I_P$ spectra. E-PL spectra were recorded with a field strength of 0.1 MV cm^{-1}. The maximum PL intensity is normalized to unity in both cases.

shown in Figure S8, Supporting Information, the magnitude of the field-induced quenching at 290 K is proportional to the square of the strength of the applied electric field, whereas that dependence deviated a little from the square law at 40 K, which might arise from a lattice distortion induced by a strong applied electric field at low temperatures. The effect of an external electric field on the photoexcitation dynamics can be discussed based on these spectra of $\Delta I_{PL}/I_{PL}$ (Figure 9b). Plots of ΔI_{PL} as a function of temperature are shown in Figure S9, Supporting Information for the intensity observed at the exciton peak and at 607 nm and for the integrated emission intensity. At temperatures above 110 K, only one emission line assigned to a free exciton is dominant. In the temperature range of 290−110 K, the extent of field-induced quenching of the PL, that is, $|\Delta I_{PL}/I_{PL}|$, increased monotonically with decreasing temperature (see Figure 7c,f). With tempearature further decreasing from 110 K, at which the emission assigned to the trap appeared, $|\Delta I_{PL}/I_{PL}|$ of a free exciton decreased with decreasing temperature. In contrast with the exciton emission, the magnitude of both the field-induced quenching, that is, $|\Delta I_{PL}/I_{PL}|$, and I_{PL} of the trap emission increased monotonically with the temperature decreasing below 110 K (Figure 7c,f and Figure S7, Supporting Information).

Since the trap emission overlaps severely with the tail of the emission spectrum of free exciton, the exact shape of the trap emission spectrum could not be identified in the PL spectra. However, the trap emission, which has a maximum at ∼607 nm, is confirmed by taking plots of $\Delta I_{PL}/I_{PL}$ as a function of wavelength at 40 K (see Figure 7c). Note that the field-induced quenching of the trap emission is much larger than that of the exciton emission having a maximum at 548 nm; the magnitudes of $\Delta I_{PL}/I_{PL}$ at 40 K with a field strength of 0.1 MV cm^{-1} was 18% for the trap emission and 10% for the exciton emission (Figure 9b). The intensity of the trap emission relative to the exciton emission depends on the sample, but trap emission is more efficiently quenched with an applied electric field in any case, as shown in Figure 9 and Figure S10, Supporting Information. It is noted that the sample of $MAPbBr_3$:QD is very stable, and E-PL spectra were reproducible, as far as the same sample was used.

Electric-field-induced quenching of PL was also observed in a two-dimensional organic−inorganic halide perovskite, $(C_4H_9NH_3)_2PbI_4$ (N1).[28] N1 showed only one exciton emission near 296 K, which was quenched with an applied electric field. At 45 K, N1 showed not only exciton emission but also trap emission, located in a wavelength region longer than that of the exciton emission band; the field-induced quenching of the trap emission of N1 was larger than that of the exciton emission. The present results of the field-induced quenching of PL of $MAPbBr_3$:QD are hence similar to those observed for N1. For N1, the field-induced decreased population of the exciton-emitting state produced on relaxation from a photoexcited state and the field-induced enhancement of the rate of nonradiative decay at the emitting state were the origin of the field-induced quenching of PL, based on the time-resolved measurements of PL decay. The field-induced quenching in $MAPbBr_3$:QD also indicates that the population of the PL emitting state is decreased on the application of an electric field and the rate of nonradiative decay at the emitting state is enhanced on the application of an electric field in $MAPbBr_3$:QD. At temperatures below 110 K, exciton emission decreased and trap emission increased with decreasing temperature, indicating that the relaxation from the photoexcited state to the trap state became more efficient with decreasing temperature. According to the results, the population of the exciton-emitting state decreased, whereas the population of the trap state increased, as the temperature decreased. The effect of an electric field on the PL indicates that relaxation from the photoexcited state to both the exciton-emitting state and the trap state becomes less efficient on the application of an electric field and the effect of the field on the relaxation to the trap state is much larger than that on the relaxation to the exciton state.

Estimation of the Binding Energy of Exciton. On assuming a Gaussian shape for the band profile, the exciton absorption band and the remaining continuum, which is assigned as a band-to-band transition, become separable. The intensity of absorption at angular frequency ω is expressible as

$$A(\omega) = A_{ex}\sum_n \frac{\sqrt{E_b}}{n^3} G1(\omega) + A_{e-h}\sum_{k=0}^{Z_{end}/h} G2(\omega) \times \frac{2\pi\sqrt{E_b}}{1 - e^{-2\pi(\sqrt{2\beta}\sqrt{E_b}/\sqrt{1-\sqrt{1-4\beta(Z_k-E_g)}})}} \frac{1}{\sqrt{1-4\beta(Z_k-E_g)}} \quad (6)$$

DOI: 10.1021/acs.jpcc.9b04567
J. Phys. Chem. C 2019, 123, 19927−19937

in which

$$G1(\omega) = e^{-((\hbar\omega-(E_g-(E_b/n^2)))^2/2\sigma^2)}$$

$$G2(\omega) = e^{-((\hbar\omega-Z_k)^2/2\sigma^2)}$$

The derivation of eq 6 was written in the Supporting Information of our previous paper (ref 34). The binding energy of free exciton of $MAPbBr_3$:QD at different temperatures was obtained in the present study with eq 6 in a similar manner to the one reported in that paper for a polycrystalline film of methylammonium lead halide perovskites including the $MAPbBr_3$ polycrystalline film. Briefly, the first and second terms in eq 6 correspond to the exciton band and the continuum band, respectively; Z_k is the kth dummy variable that has an equally spaced energy of ~0.81 cm^{-1}, β represents the magnitude of nonparabolicity of the band dispersion, E_b is the binding energy of the exciton (electron−hole pair), E_g is the band-gap energy, and the relation $E_g = \hbar\nu_0 + E_b$ holds for the exciton band. Here, $\hbar\nu_0$ is the energy of the exciton band. As a lineshape function, we used Gaussian functions for $G1$ and $G2$, because this shape was assumed in deriving the absorption spectrum of the exciton band in the analysis of the E-A spectra. σ in eq 6 was estimated from the full width at half-maximum (FWHM) of the exciton band. To simulate the observed absorption spectrum as a combination of exciton band and continuum band, we used the same FWHM and center of the exciton band (ν_0) that were extracted with the integral method from the E-A spectra (see Figure 5 and Figures S3−S6, Supporting Information). In the simulation, the total absorption spectrum was well reproduced with eq 6 with suitable values of parameters E_b, β, and A_{ex}/A_{e-h}. The results at 290 and 40 K are shown in Figure 10. The results at

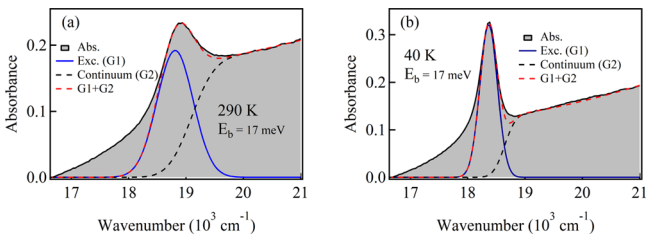

Figure 10. Absorption spectra of $MAPbBr_3$:QD doped in a PMMA film at (a) 290 K and (b) 40 K. The shaded line shows the recorded spectra, and a red line shows the simulated absorption spectrum given as a sum of the exciton band (G1, blue solid line) and continuum (G2, black dashed line) that were simulated with eq 6. The parameters used in the simulation are shown in Table S1, Supporting Information.

other temperatures between 290 and 40 K are shown in Figure S11, Supporting Information. The parameters used in the simulation are listed in Table S1, Supporting Information. In the results, the binding energy of the exciton (E_b) of $MAPbBr_3$:QD has been determined to be 17 ± 1 meV, irrespective of the temperature.

The binding energy of $MAPbBr_3$:QD was also estimated from the temperature-dependent PL intensities. In the relaxation of an exciton, only the dissociation, of which the rate constant is given by k_{dis}, is assumed to depend on the temperature. The rate constant (k_{ex}) for the exciton decay is expressed as $k_{ex} = k_r + k_{nr} + k_{dis}\exp(-E_b/k_BT)$, in which k_r and k_{nr} are the temperature-independent radiative and nonradiative decay rate constants, respectively, and k_B is the Boltzmann constant. As the emission quantum yield is given by k_r/k_{ex}, the inverse of the quantum yield of PL, $1/\Phi(T)$, as a function of temperature is expressible as

$$\frac{1}{\Phi(T)} = \frac{1}{\Phi(T=0)} + \frac{k_{dis}}{k_r}\exp\left(-\frac{E_b}{k_BT}\right) \quad (7)$$

In the temperaure range of 150−290 K, only the exciton emission is dominant; the emission intensity increased monotonically with decreasing temperature, as shown in Figure S7, Supporting Information. The binding energy of E_b was then estimated on fitting the PL intensity in this temperature range with the equation

$$\frac{1}{I(T)} = A + B\exp\left(-\frac{E_b}{k_BT}\right) \quad (8)$$

where A and B are the fitting parameters; parameter A corresponds to the inverse of the PL intensity at T = 0 K. If the emission quantum yield is used in eq 8 instead of $I(T)$, parameters A and B corrrespond to the inverse of the emission quantum yield at 0 K and k_{dis}/k_r, respectively (see eq 7). As shown in Figure 11, the temperature dependence of $I(T)$ is

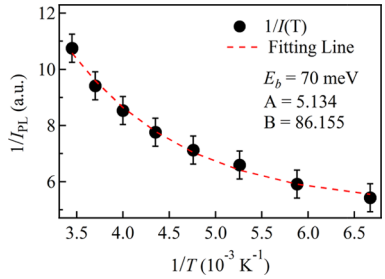

Figure 11. Inverse of the PL intensity of $MAPbBr_3$:QD doped in a PMMA film as a function of the inverse of temperature. The simulation with eq 8 is shown as a red line.

well fitted with eq 8; the binding energy is estimated to be ~70 meV. In the fit, product $AI(T)$, which corresponds to $I(T)/I(T = 0)$, is determined to be 0.478 at T = 290 K. As the temperature increases from 0 to 290 K, only half the emission intensity thus decreases.

The binding energy of an exciton of $MAPbBr_3$:QD was estimated from the absorption spectra to be ~17 meV, as already mentioned. The binding energy estimated from the temperature dependence of PL intensity is about twice that estimated from the absorption spectra. These results indicate that the exciton directly produced following absorption and the exciton that produces PL have distinct binding energies. Woo et al. reported that the binding energy of quantum dots of $MAPbBr_3$ (388.2 meV) was much larger that that of a polycrystalline thin film (124.4 meV) or a single crystal (40.6 meV) based on the temperature dependence of the PL intensity.[26] Zheng et al. also reported a large binding energy of QD of $MAPbBr_3$, that is, 320 meV based on the X-ray spectra.[56] The binding energy of $MAPbBr_3$:QD derived from the temperature-dependent PL intensity in the present work is much smaller than their binding energy of the quantum dots, even smaller than the value in a polycrystalline thin film. Regarding the binding energy estimated from the absorption profile, the value for $MAPbBr_3$:QD, that is, 17 meV is roughly the same as that estimated for a polycrystaline thin film, that is,

DOI: 10.1021/acs.jpcc.9b04567
J. Phys. Chem. C 2019, 123, 19927−19937

14 meV.[34] The large binding energy of the exciton emitting state in QD might be a significant reason for a large emission quantum yield, but the present result shows that the binding energy for QD estimated by Woo et al. or Zheng et al. was too large. Even for a binding energy of 70 meV, as estimated in the present work from the temperature-dependent PL, only half the PL intensity is quenched by the exciton dissociation with the temperature increasing from 0 to 300 K. The present results show that the emission quantum yield can be large even when the binding energy of an emitting exciton is not large. For a polycrystaline thin film or a single crystal, another possibility such as large exciton−phonon scattering might have to be considered as the origin of their small emission quantum yield near 296 K, in comparison with the quantum yield of QD of $MAPbBr_3$.

CONCLUSIONS

Temperature-dependent absorption, E-A, PL, and E-PL spectra of $MAPbBr_3$:QD doped in a PMMA film have been recorded at temperatures in the range of 40−290 K. A frequency-dependent field-induced variation of absorption intensity has been observed; ion migration that follows the modulation of the applied electric filed has been confirmed at frequencies less than 500 Hz. A comparison of the results at 40 and 290 K indicates that the field-induced ion migration becomes more efficient with increasing temperature. The E-A spectra recorded at temperatures in the range of 40−290 K have been analyzed with an integral method on assuming that the E-A signal resulted from the Stark shift; the magnitudes of $\Delta\bar{\alpha}$ and $|\Delta\boldsymbol{\mu}|$ following absorption have been evaluated at each temperature. Both values depend strongly on the temperature, likely because of a temperature-dependent lattice deformation. According to an analysis of the absorption profile, the binding energy of an exciton was estimated to be ∼17 meV, indicating that the binding energy of $MAPbBr_3$:QD is nearly the same as the exciton binding energy of a polycrystalline thin film of $MAPbBr_3$ estimated from the absorption profile. The binding energy of an exciton of $MAPbBr_3$:QD at the emitting state estimated from the temperature-dependent PL intensity is ∼70 meV, which is much larger than that estimated from the absorption spectra. The E-PL spectra show that the PL of $MAPbBr_3$:QD is quenched on the application of an electric field at each temperature. At temperatures below 110 K, both exciton emission and trap emission were observed. The trap emission, which has a maximum at ∼607 nm, was more efficiently quenched on the application of an electric field than the exciton emission. Exciton−phonon interaction is considered to be responsible for the linewidth broadening of the PL spectra.

ASSOCIATED CONTENT

Supporting Information

The Supporting Information is available free of charge on the ACS Publications website at DOI: 10.1021/acs.jpcc.9b04567.

TEM image of a single quantum dot of $MAPbBr_3$, temperature dependence of band-gap energy, integral method analysis of E-A spectra at various temperatures, temperature dependence of PL intensity, field strength dependence of E-PL signal, temperature dependence of E-PL signal, sample dependence of E-PL spectra at 40 K, simulation of absorption spectra to determine the binding energy of an exciton at varied temperatures, and fitted parameters used for the theoretical simulation of absorption profile (PDF)

AUTHOR INFORMATION

Corresponding Authors

*E-mail: diau@mail.nctu.edu.tw (E.W.-G.D.).
*E-mail: nohta@nctu.edu.tw (N.O.).

ORCID

Kamlesh Awasthi: 0000-0001-7852-059X
Eric Wei-Guang Diau: 0000-0001-6113-5679
Nobuhiro Ohta: 0000-0003-4255-6448

Notes

The authors declare no competing financial interest.

ACKNOWLEDGMENTS

Ministry of Science and Technology (MOST) in Taiwan provided the financial support of this research (MOST 107-2113-M-009-005, MOST 108-2113-M-009-002, MOST 107-3017-F009-003, and MOST 105-2119-M-009-011-MY3). This work was also financially supported by the Center for Emergent Functional Matter Science of National Chiao Tung University from The Featured Areas Research Center Program within the framework of the Higher Education SPROUT Project by the Ministry of Education (MOE) in Taiwan.

REFERENCES

(1) Cui, D.; Yang, Z.; Yang, D.; Ren, X.; Liu, Y.; Wei, Q.; Fan, H.; Zeng, J.; Liu, S. Color-Tuned Perovskite Films Prepared for Efficient Solar Cell Applications. *J. Phys. Chem. C* **2015**, *120*, 42−47.

(2) Zhou, Z.; Pang, S.; Liu, Z.; Xu, H.; Cui, G. Interface Engineering for High-Performance Perovskite Hybrid Solar Cells. *J. Mater. Chem. A* **2015**, *3*, 19205−19217.

(3) Yoo, E. J.; Lyu, M.; Yun, J.-H.; Kang, C. J.; Choi, Y. J.; Wang, L. Resistive Switching Behavior in Organic-Inorganic Hybrid $CH_3NH_3PbI_{3-x}Cl_x$ Perovskite for Resistive Random Access Memory Devices. *Adv. Mater.* **2015**, *27*, 6170−6175.

(4) Gu, C.; Lee, J.-S. Flexible Hybrid Organic-Inorganic Perovskite Memory. *ACS Nano* **2016**, *10*, 5413−5418.

(5) Hu, X.; Zhang, X.; Liang, L.; Bao, J.; Li, S.; Yang, W.; Xie, Y. High-Performance Flexible Broadband Photodetector Based on Organolead Halide Perovskite. *Adv. Funct. Mater.* **2014**, *24*, 7373−7380.

(6) Stranks, S. D.; Hoye, R. L. Z.; Di, D.; Friend, R. H.; Deschler, F. The Physics of Light Emission in Halide Perovskite Devices. *Adv. Mater.* **2018**, 1803336.

(7) Kirchartz, T.; Staub, F.; Rau, U. Impact of Photon Recycling on the Open-Circuit Voltage of Metal Halide Perovskite Solar Cells. *ACS Energy Lett.* **2016**, *1*, 731−739.

(8) Richter, J. M.; Abdi-Jalebi, M.; Sadhanala, A.; Tabachnyk, M.; Rivett, J. P. H.; Pazos-Outón, L. M.; Gödel, K. C.; Price, M.; Deschler, F.; Friend, R. H. Enhancing Photoluminescence Yields in Lead Halide Perovskites by Photon Recycling and Light Out-Coupling. *Nat. Commun.* **2016**, *7*, 13941.

(9) Kulkarni, S. A.; Baikie, T.; Boix, P. P.; Yantara, N.; Mathews, N.; Mhaisalkar, S. Band-Gap Tuning of Lead Halide Perovskites Using a Sequential Deposition Process. *J. Mater. Chem. A* **2014**, *2*, 9221−9225.

(10) Zhang, F.; Zhong, H.; Chen, C.; Wu, X.-g.; Hu, X.; Huang, H.; Han, J.; Zou, B.; Dong, Y. Brightly Luminescent and Color-Tunable Colloidal $CH_3NH_3PbX_3$ (X = Br, I, Cl) Quantum Dots: Potential Alternatives for Display Technology. *ACS Nano* **2015**, *9*, 4533−4542.

(11) Zhang, M.; Yu, H.; Lyu, M.; Wang, Q.; Yun, J.-H.; Wang, L. Composition-Dependent Photoluminescence Intensity and Prolonged

DOI: 10.1021/acs.jpcc.9b04567
J. Phys. Chem. C 2019, 123, 19927−19937

Recombination Lifetime of Perovskite $CH_3NH_3PbBr_{3-x}Cl_x$ films. *Chem. Commun.* **2014**, *50*, 11727−11730.
(12) Frost, J. M.; Butler, K. T.; Brivio, F.; Hendon, C. H.; van Schilfgaarde, M.; Walsh, A. Atomistic Origins of High-Performance in Hybrid Halide Perovskite Solar Cells. *Nano Lett.* **2014**, *14*, 2584−2590.
(13) Li, Y.; Shi, Z.; Lei, L.; Ma, Z.; Zhang, F.; Li, S.; Wu, D.; Xu, T.; Li, X.; Shan, C.; Du, G. Controllable Vapor-Phase Growth of Inorganic Perovskite Microwire Networks for High-Efficiency and Temperature-Stable Photodetectors. *ACS Photonics* **2018**, *5*, 2524−2532.
(14) Pisoni, A.; Jaćimović, J.; Barišić, O. S.; Spina, M.; Gaál, R.; Forró, L.; Horváth, E. Ultra-Low Thermal Conductivity in Organic−Inorganic Hybrid Perovskite $CH_3NH_3PbI_3$. *J. Phys. Chem. Lett.* **2014**, *5*, 2488−2492.
(15) Yuan, Y.; Chae, J.; Shao, Y.; Wang, Q.; Xiao, Z.; Centrone, A.; Huang, J. Photovoltaic Switching Mechanism in Lateral Structure Hybrid Perovskite Solar Cells. *Adv. Energy Mater.* **2015**, *5*, 1500615.
(16) Bae, S.; Kim, S.; Lee, S.-W.; Cho, K. J.; Park, S.; Lee, S.; Kang, Y.; Lee, H.-S.; Kim, D. Electric-Field-Induced Degradation of Methylammonium Lead Iodide Perovskite Solar Cells. *J. Phys. Chem. Lett.* **2016**, *7*, 3091−6.
(17) Schmidt, L. C.; Pertegás, A.; González-Carrero, S.; Malinkiewicz, O.; Agouram, S.; Mínguez Espallargas, G.; Bolink, H. J.; Galian, R. E.; Pírez-Prieto, J. Nontemplate Synthesis of $CH_3NH_3PbBr_3$ Perovskite Nanoparticles. *J. Am. Chem. Soc.* **2014**, *136*, 850−3.
(18) Chen, Q.; De Marco, N.; Yang, Y.; Song, T.-B.; Chen, C.-C.; Zhao, H.; Hong, Z.; Zhou, H.; Yang, Y. Under the Spotlight: the Organic−Inorganic Hybrid Halide Perovskite for Optoelectronic Applications. *Nano Today* **2015**, *10*, 355−396.
(19) Huang, H.; Xue, Q.; Chen, B.; Xiong, Y.; Schneider, J.; Zhi, C.; Zhong, H.; Rogach, A. L. Top-Down Fabrication of Stable Methylammonium Lead Halide Perovskite Nanocrystals by Employing a Mixture of Ligands as Coordinating Solvents. *Angew. Chem., Int. Ed.* **2017**, *56*, 9571−9576.
(20) Chen, L.-C.; Lee, K.-L.; Huang, C.-Y.; Lin, J.-C.; Tseng, Z.-L. Preparation and Characteristics of $MAPbBr_3$ Perovskite Quantum Dots on NiO_x Film and Application for High Transparent Solar Cells. *Micromachines* **2018**, *9*, 205.
(21) Mali, S. S.; Shim, C. S.; Hong, C. K. Highly Stable and Efficient Solid-state Solar Cells Based on Methylammonium Lead Bromide ($CH_3NH_3PbBr_3$) Perovskite Quantum Dots. *NPG Asia Mater.* **2015**, *7*, No. e208.
(22) Deng, W.; Fang, H.; Jin, X.; Zhang, X.; Zhang, X.; Jie, J. Organic−Inorganic Hybrid Perovskite Quantum Dots for Light-emitting Diodes. *J. Mater. Chem. C* **2018**, *6*, 4831−4841.
(23) Yang, K.; Li, F.; Veeramalai, C. P.; Guo, T. A Facile Synthesis of $CH_3NH_3PbBr_3$ Perovskite Quantum Dots and Their Application in Flexible Nonvolatile Memory. *Appl. Phys. Lett.* **2017**, *110*, No. 083102.
(24) Zhang, Z.-Y.; Wang, H.-Y.; Zhang, Y.-X.; Hao, Y.-W.; Sun, C.; Zhang, Y.; Gao, B.-R.; Chen, Q.-D.; Sun, H.-B. The Role of Trap-Assisted Recombination in Luminescent Properties of Organometal Halide $CH_3NH_3PbBr_3$ Perovskite Films and Quantum Dots. *Sci. Rep.* **2016**, *6*, 27286.
(25) Luo, B.; Pu, Y.-C.; Yang, Y.; Lindley, S. A.; Abdelmageed, G.; Ashry, H.; Li, Y.; Li, X.; Zhang, J. Z. Synthesis, Optical Properties, and Exciton Dynamics of Organolead Bromide Perovskite Nanocrystals. *J. Phys. Chem. C* **2015**, *119*, 26672−26682.
(26) Woo, H. C.; Choi, J. W.; Shin, J.; Chin, S.-H.; Ann, M. H.; Lee, C.-L. Temperature-Dependent Photoluminescence of $CH_3NH_3PbBr_3$ Perovskite Quantum Dots and Bulk Counterparts. *J. Phys. Chem. Lett.* **2018**, *9*, 4066−4074.
(27) Amerling, E.; Baniya, S.; Lafalce, E.; Zhang, C.; Vardeny, Z. V.; Whittaker-Brooks, L. Electroabsorption Spectroscopy Studies of $(C_4H_9NH_3)_2PbI_4$ Organic-Inorganic Hybrid Perovskite Multiple Quantum Wells. *J. Phys. Chem. Lett.* **2017**, *8*, 4557−4564.
(28) Kattoor, V.; Awasthi, K.; Jokar, E.; Diau, E. W.-G.; Ohta, N. Integral Method Analysis of Electroabsorption Spectra and Electrophotoluminescence Study of $(C_4H_9NH_3)_2PbI_4$ Organic−Inorganic Quantum Well. *J. Phys. Chem. C* **2018**, *122*, 26623−26634.
(29) Xiao, G.; Cao, Y.; Qi, G.; Wang, L.; Liu, C.; Ma, Z.; Yang, X.; Sui, Y.; Zheng, W.; Zou, B. Pressure Effects on Structure and Optical Properties in Cesium Lead Bromide Perovskite Nanocrystals. *J. Am. Chem. Soc.* **2017**, *139*, 10087−10094.
(30) Ma, Z.; Liu, Z.; Lu, S.; Wang, L.; Feng, X.; Yang, D.; Wang, K.; Xiao, G.; Zhang, L.; Redfern, S. A. T.; Zou, B. Pressure-Induced Emission of Cesium Lead Halide Perovskite Nanocrystals. *Nat. Commun.* **2018**, *9*, 4506.
(31) Leijtens, T.; Srimath Kandada, A. R.; Eperon, G. E.; Grancini, G.; D'Innocenzo, V.; Ball, J. M.; Stranks, S. D.; Snaith, H. J.; Petrozza, A. Modulating the Electron-Hole Interaction in a Hybrid Lead Halide Perovskite with an Electric Field. *J. Am. Chem. Soc.* **2015**, *137*, 15451−15459.
(32) Ohta, N.; Awasthi, K.; Okoshi, K.; Manseki, K.; Miura, H.; Inoue, Y.; Nakamura, E.; Kono, H.; Diau, E. W.-G. Stark Spectroscopy of Absorption and Emission of Indoline Sensitizers: A Correlation with the Performance of Photovoltaic Cells. *J. Phys. Chem. C* **2016**, *120*, 26206−26216.
(33) Awasthi, K.; Wang, C.-Y.; Fathi, A.; Narra, S.; Diau, E. W.-G.; Ohta, N. Anisotropic Electric Field Effect on the Photoluminescence of $CH_3NH_3PbI_3$ Perovskite Sandwiched between Conducting and Insulating Films. *J. Phys. Chem. C* **2017**, *121*, 22700−22706.
(34) Awasthi, K.; Du, K.-B.; Wang, C.-Y.; Tsai, C.-L.; Hamada, M.; Narra, S.; Diau, E. W.-G.; Ohta, N. Electroabsorption Studies of Multicolored Lead Halide Perovskite Nanocrystalline Solid Films. *ACS Photonics* **2018**, *5*, 2408−2417.
(35) Umeuchi, S.; Nishimura, Y.; Yamazaki, I.; Murakami, H.; Yamashita, M.; Ohta, N. Electric-field Effects on Absorption and Fluorescence Spectra of Pyrene Doped in a PMMA Polymer Film. *Thin Solid Films* **1997**, *311*, 239−245.
(36) Elbaz, G. A.; Straus, D. B.; Semonin, O. E.; Hull, T. D.; Paley, D. W.; Kim, P.; Owen, J. S.; Kagan, C. R.; Roy, X. Unbalanced Hole and Electron Diffusion in Lead Bromide Perovskites. *Nano Lett.* **2017**, *17*, 1727−1732.
(37) Fujita, M.; Itoh, M.; Bokumoto, Y.; Nakagawa, H.; Alov, D. L.; Kitaura, M. Optical Spectra and Electronic Structures of Lead Halides. *Phys. Rev. B* **2000**, *61*, 15731−15737.
(38) Lee, S. M.; Moon, C. J.; Lim, H.; Lee, Y.; Choi, M. Y.; Bang, J. Temperature-Dependent Photoluminescence of Cesium Lead Halide Perovskite Quantum Dots: Splitting of the Photoluminescence Peaks of $CsPbBr_3$ and $CsPb(Br/I)_3$ Quantum Dots at Low Temperature. *J. Phys. Chem. C* **2017**, *121*, 26054−26062.
(39) Gibbs, Z. M.; Kim, H.; Wang, H.; White, R. L.; Drymiotis, F.; Kaviany, M.; Jeffrey Snyder, G. Temperature Dependent Band Gap in PbX (X = S, Se, Te). *Appl. Phys. Lett.* **2013**, *103*, 262109.
(40) Wright, A. D.; Verdi, C.; Milot, R. L.; Eperon, G. E.; Pírez-Osorio, M. A.; Snaith, H. J.; Giustino, F.; Johnston, M. B.; Herz, L. M. Electron−phonon Coupling in Hybrid Lead Halide Perovskites. *Nat. Commun.* **2016**, *7*, 11755.
(41) D'Innocenzo, V.; Grancini, G.; Alcocer, M. J. P.; Kandada, A. R. S.; Stranks, S. D.; Lee, M. M.; Lanzani, G.; Snaith, H. J.; Petrozza, A. Excitons Versus Free Charges in Organo-Lead Tri-Halide Perovskites. *Nat. Commun.* **2014**, *5*, 3586.
(42) Chen, C.; Hu, X.; Lu, W.; Chang, S.; Shi, L.; Li, L.; Zhong, H.; Han, J.-B. Elucidating the Phase Transitions and Temperature-dependent Photoluminescence of $MAPbBr_3$ Single Crystal. *J. Phys. D: Appl. Phys.* **2018**, *51*, No. 045105.
(43) Liu, Y.; Lu, H.; Niu, J.; Zhang, H.; Lou, S.; Gao, C.; Zhan, Y.; Zhang, X.; Jin, Q.; Zheng, L. Temperature-dependent Photoluminescence Spectra and Decay Dynamics of $MAPbBr_3$ and $MAPbI_3$ thin films. *AIP Adv.* **2018**, *8*, No. 095108.
(44) Varshni, Y. P. Temperature Dependence of the Energy Gap in Semiconductors. *Physica* **1967**, *34*, 149−154.
(45) Chon, B.; Bang, J.; Park, J.; Jeong, C.; Choi, J. H.; Lee, J.-B.; Joo, T.; Kim, S. Unique Temperature Dependence and Blinking

DOI: 10.1021/acs.jpcc.9b04567
J. Phys. Chem. C 2019, 123, 19927−19937

Behavior of CdTe/CdSe (core/shell) Type-II Quantum Dots. *J. Phys. Chem. C* **2010**, *115*, 436−442.
(46) Swarnkar, A.; Ravi, V. K.; Nag, A. Beyond Colloidal Cesium Lead Halide Perovskite Nanocrystals: Analogous Metal Halides and Doping. *ACS Energy Lett.* **2017**, *2*, 1089−1098.
(47) Ishikawa, K. Electric Field Effect on the Absorption Edge in SBSI. *Jpn. J. Appl. Phys.* **1980**, *19*, 1301−1309.
(48) Liptay, W. Dipole Moments and Polariabilities of Molecules in Excited Electronic States. In *Excited States*; Lim, E. C., Ed.; Elsevier: New York USA, 1974; Vol. *1*, pp 129−229.
(49) Bublitz, G. U.; Boxer, S. G. Stark Spectroscopy: Applications in Chemistry, Biology, and Materials Science. *Ann. Rev. Phys. Chem.* **1997**, *48*, 213−242.
(50) Locknar, S. A.; Peteanu, L. A. Investigation of the Relationship Between Dipolar Properties and Cis−trans Configuration in Retinal Polyenes: a Comparative Study Using Stark Spectroscopy and Semiempirical Calculations. *J. Phys. Chem. B* **1998**, *102*, 4240−4246.
(51) Jalviste, E.; Ohta, N. Theoretical Foundation of Electro-absorption Spectroscopy: Self-Contained Derivation of the Basic Equations with the Direction Cosine Method and the Euler Angle Method. *J. Photochem. Photobiol. C* **2007**, *8*, 30−46.
(52) Awasthi, K.; Iimori, T.; Ohta, N. Integral Method Analysis of Electroabsorption Spectra and Its Application to Quantum Dots of PbSe. *J. Phys. Chem. C* **2014**, *118*, 18170−18176.
(53) Awasthi, K.; Iimori, T.; Ohta, N. Electroabsorption Spectra of Quantum Dots of PbS and Analysis by the Integral Method. *J. Phys. Chem. C* **2015**, *119*, 4351−4361.
(54) Rudin, S.; Reinecke, T. L.; Segall, B. Temperature-Dependent Exciton Linewidths in Semiconductors. *Phys. Rev. B* **1990**, *42*, 11218−11231.
(55) Ni, L.; Huynh, U.; Cheminal, A.; Thomas, T. H.; Shivanna, R.; Hinrichsen, T. F.; Ahmad, S.; Sadhanala, A.; Rao, A. Real-Time Observation of Exciton−phonon Coupling Dynamics in Self-Assembled Hybrid Perovskite Quantum Wells. *ACS Nano* **2017**, *11*, 10834−10843.
(56) Zheng, K.; Zhu, Q.; Abdellah, M.; Messing, M. E.; Zhang, W.; Generalov, A.; Niu, Y.; Ribaud, L.; Canton, S. E.; Pullerits, T. Exciton Binding Energy and the Nature of Emissive States in Organometal Halide Perovskites. *J. Phys. Chem. Lett.* **2015**, *6*, 2969−2975.

DOI: 10.1021/acs.jpcc.9b04567
J. Phys. Chem. C 2019, 123, 19927−19937